ARTICLE

doi:10.1038/nature09450

Video imaging of walking myosin V by high-speed atomic force microscopy

Noriyuki Kodera[1,2], Daisuke Yamamoto[1,2], Ryoki Ishikawa[3] & Toshio Ando[1,2]

The dynamic behaviour of myosin V molecules translocating along actin filaments has been mainly studied by optical microscopy. The processive hand-over-hand movement coupled with hydrolysis of adenosine triphosphate was thereby demonstrated. However, the protein molecules themselves are invisible in the observations and have therefore been visualized by electron microscopy in the stationary states. The concomitant assessment of structure and dynamics has been unfeasible, a situation prevailing throughout biological research. Here we directly visualize myosin V molecules walking along actin tracks, using high-speed atomic force microscopy. The high-resolution movies not only provide corroborative 'visual evidence' for previously speculated or demonstrated molecular behaviours, including lever-arm swing, but also reveal more detailed behaviours of the molecules, leading to a comprehensive understanding of the motor mechanism. Our direct and dynamic high-resolution visualization is a powerful new approach to studying the structure and dynamics of biomolecules in action.

Proteins are dynamic in nature and work at the single-molecule level. Reflecting this fact, single-molecule fluorescence microscopy has been widely exploited to understand how proteins operate (reviewed in ref. 1). However, what we can observe thereby is the dynamic behaviour of individual fluorescent spots (each being emitted from a fluorophore attached to a selected locus of the molecule), not of the protein molecules themselves. The structure of proteins has been studied by electron microscopy, X-ray crystallography and NMR, but the obtained structures are essentially static. To overcome this long-standing problem and make it possible to record the structure and dynamics of functioning biomolecules simultaneously, high-speed atomic force microscopy (HS-AFM) has been developed[2–5]. The recent significant improvement in its performance has been demonstrated in a few imaging studies of proteins[6–8].

Myosin V is a two-headed processive motor and functions as a cargo transporter in cells (reviewed in ref. 9). Facilitated by the processivity of the molecule[10,11], numerous single-molecule studies have demonstrated that it moves hand over hand with a ~36-nm advance[12,13] for every adenosine triphosphate (ATP) hydrolysis[14]. However, a comprehensive description of the molecule in action has not yet been attained. We applied HS-AFM to this highly dynamic protein to capture its minute dynamic behaviours. In addition to known and speculated behaviours, previously unappreciated ones clearly appeared in the molecular movies: 'stomping-like' brief detachment and rebinding of either head; occasional unwinding of the coiled-coil tail of the two-headed bound molecule followed by the leading lever-arm swing, indicating the presence of intramolecular tension responsible for the power stroke; and repeated conformational switching of the leading head by adenosine diphosphate (ADP) binding and release. These findings lead to a better understanding of how myosin V operates for its motor function.

Unidirectional processive movement

Partially biotinylated actin filaments were immobilized using streptavidin with a low surface density on biotin-containing lipid bilayers formed on a mica surface (Supplementary Fig. 1). To facilitate the weak sideways adsorption of tail-truncated myosin V (M5-HMM) onto the bilayer surface, a positively charged lipid (1,2-dipalmitoyl-3-trimethylammonium-propane (DPTAP), 5%) was included in the bilayer unless otherwise stated. This condition was necessary to clearly visualize M5-HMM molecules.

Figure 1a shows images of M5-HMM moving processively with discrete ~36-nm steps (Supplementary Movie 1). A processive run almost always continued to the full extent of each imaging range used (that is, 4–16 steps). Typical long runs tracked by shifting the scan area are shown in Supplementary Movie 1c, d. In the two-headed bound M5-HMM (where by head we mean the motor domain and the neck domain), the neck–motor domain junction appears smooth in the leading head (L-head) but is V-shaped in the trailing head (T-head) without exception (Fig. 1b), because the neck regions emerge from different parts of the motor domain. The short coiled-coil tail was mostly tilted towards the minus end of actin (Fig. 1a, arrows). These features are consistent with electron microscopy observations[15–17] and can be used to determine the actin polarity when bound M5-HMM is stationary.

The average translocation velocity (V) as a function of ATP concentration ([ATP]) was well fitted by $V = d_s(1/k_1[\mathrm{ATP}] + 1/k_2)^{-1}$, where d_s is the step size, k_1 is the second-order ATP binding rate constant and k_2 is the first-order ADP dissociation rate constant (Supplementary Fig. 2). The maximum velocity observed without DPTAP was similar to that measured by fluorescence microscopy[13,18], indicating the negligible effects of the tip–sample and surface–sample interactions on motor activity. When 5% DPTAP was included in the substrate surface, the values $k_1 = 0.9 \pm 0.3\,\mu\mathrm{M}^{-1}\,\mathrm{s}^{-1}$ and $k_2 = 7.2 \pm 1.5\,\mathrm{s}^{-1}$ were obtained (Supplementary Table 1). The former agrees with previous reports, but the latter is about 70% of previously reported values[13,18] ($\sim 11\,\mathrm{s}^{-1}$), suggesting that the surface–sample interaction slightly reduces the rate of ADP release from the T-head.

Hand-over-hand movement

As observed above, the ~36-nm advance was completed within one frame (146.7 ms); therefore, the molecular process occurring during a

[1]Department of Physics, Kanazawa University, Kakuma-machi, Kanazawa 920-1192, Japan. [2]CREST, JST, Sanban-cho, Chiyoda-ku, Tokyo 102-0075, Japan. [3]Department of Molecular and Cellular Pharmacology, Gunma University Graduate School of Medicine, 3-39-22 Showa-machi, Maebashi 371-8511, Japan.

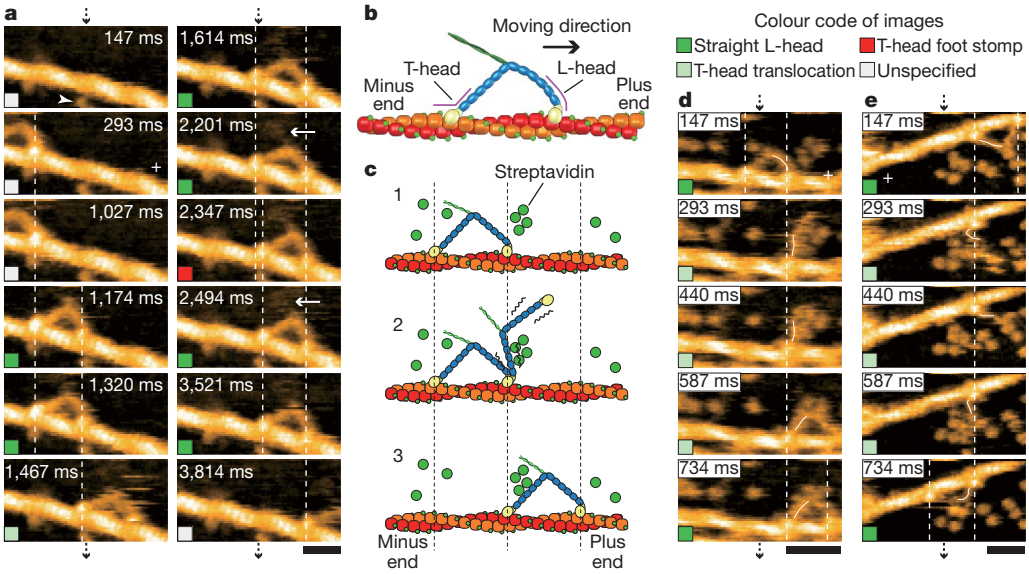

Figure 1 | Directly visualized walking M5-HMM. **a**, Successive AFM images showing processive movement of M5-HMM in 1 μM ATP (Supplementary Movie 1). Arrowhead, streptavidin molecule; arrows, coiled-coil tail of M5-HMM tilted towards the minus end of actin. Scan area, 130 × 65 nm^2; scale bar, 30 nm. **b**, Schematic of two-headed bound M5-HMM. **c**, Schematic explaining the images in **d** and **e**. **d**, **e**, Successive AFM images showing hand-over-hand movement in 1 μM ATP (**d**; scan area, 150 × 75 nm^2; scale bar, 50 nm) and in 2 μM ATP (**e**; scan area, 130 × 65 nm^2; scale bar, 30 nm) (Supplementary Movie 2). The swinging lever is highlighted with a thin white line. Vertical dashed lines in **a**, **d** and **e** show the centres of mass of the motor domains, and a plus sign is used to indicate the plus end of actin. All images were taken at a 146.7 ms per frame.

step could not be resolved. However, additional streptavidin molecules placed on the substrate surface as moderate obstacles to the advance allowed the visualization of this process (Fig. 1c–e). After T-head detachment, the nearly straight leading neck swung from the reverse arrowhead (R-ARH) orientation to the arrowhead (ARH) orientation (Supplementary Movie 2), confirming the swinging lever-arm motion initially proposed for muscle myosin[19]. The detached T-head rotationally diffused around the advancing neck–neck junction (no translational diffusion on the actin occurs; Supplementary Movie 2c) and then bound to a forward site on the actin filament, completing one step. Thus, the hand-over-hand movement[12,13], including the intermediate process, was directly visualized at high resolution. We did not observe other behaviours of M5-HMM predicted by the 'inchworm'[20] and 'biased diffusion'[21] models, at least with the time resolution used. The captured images show that the forward movement is driven not by bending but by rotation of the L-head. The rotation seems to occur spontaneously after T-head detachment, suggesting that intramolecular tension driving the L-head swing exists in the two-headed bound molecules.

Unfolding of the coiled-coil tail

In a saturating amount of ADP, both heads were bound to a single actin filament and the L-head always appeared nearly straight (curved slightly outwards; Fig. 2a, Supplementary Movie 3 and Supplementary Fig. 3b), as observed for M5-HMM moving in 0.1 μM and 1 μM ATP. In this nearly straight conformation, the neck domain appears to emerge from the rear of the motor domain[17]. During imaging of the two-headed bound M5-HMM, we sometimes encountered unwinding of the short coiled-coil tail. After unwinding, the monomerized L-head immediately rotated towards the ARH orientation (Fig. 2b and Supplementary Movie 4). This head separation was rarely reversed (Supplementary Movie 4c, d). This unwinding is unlikely to be caused by the tip–sample interaction because monomeric heads were detected in the earliest frames in the successive movies in new scan areas (see the latter half of Supplementary Movie 4b), and because a previous study showed the presence of a single-head fragment with an intact coiled-coil region in an expressed M5-HMM sample, although it was interpreted to be due to partial proteolysis[22]. Rather, this finding directly demonstrates that intramolecular tension exists in the two-headed bound M5-HMM, and that the tension release caused by the unwinding results in the L-head rotation, similar to the L-head behaviour in the hand-over-hand movement. These observations provide the following insights into the motor mechanism: first, the neck–motor domain junction of L-head–ADP is sufficiently flexible to allow the head to bind strongly to actin in the R-ARH orientation, even without transitioning through a weak-binding ADP–P_i-bound state (P_i, inorganic phosphate); second, this strong binding forces the L-head into a strained 'pre-stroke' state; and third, the rotation of the L-head is likely to occur spontaneously when the constraint holding it in the strained state is removed by T-head detachment, suggesting that the lever swing by the L-head is not accompanied by chemical transitions there.

Foot stomp in ATP

In general, during the actomyosin ATPase cycle, the strained pre-stroke state is always formed after P_i is released from an ADP–P_i-bound head weakly interacting with actin[23]. Thus, it may be considered that the strained pre-stroke state, which is formed directly by the binding of L-head–ADP to actin, does not participate in the forward step. However, we observed molecular behaviour in ATP that indicates that it does participate. In two-headed bound M5-HMM, both of the motor domains frequently exhibited brief dissociation and reassociation on the same actin filament (or a brief translocation by around ±5 nm along the actin filament), whereas M5-HMM remained at approximately the same position on the filament (Fig. 1, Supplementary Fig. 3a, Supplementary Movies 1 and 2, and Methods). We have termed this behaviour 'foot stomp'. Note that when the T-head dissociates, it rarely rebinds to actin without stepping forward; thus, the T-head foot stomp is usually observed as a brief translocation along the actin filament. The foot stomp was more frequently observed at the L-head than at the T-head (by a ratio of approximately 3:1; Fig. 3a). The briefly detached L-head does not carry bound P_i because P_i is rapidly released from an ADP–P_i-bound head when it attaches to actin[24]. Nevertheless, the detached L-head with only ADP bound rebinds to actin, still in the R-ARH orientation, and then swings forward following T-head detachment.

At each step, the L-head foot stomp occurred about twice in 0.1 μM ATP and 0.4 times in 1 μM ATP on average. These high frequencies of

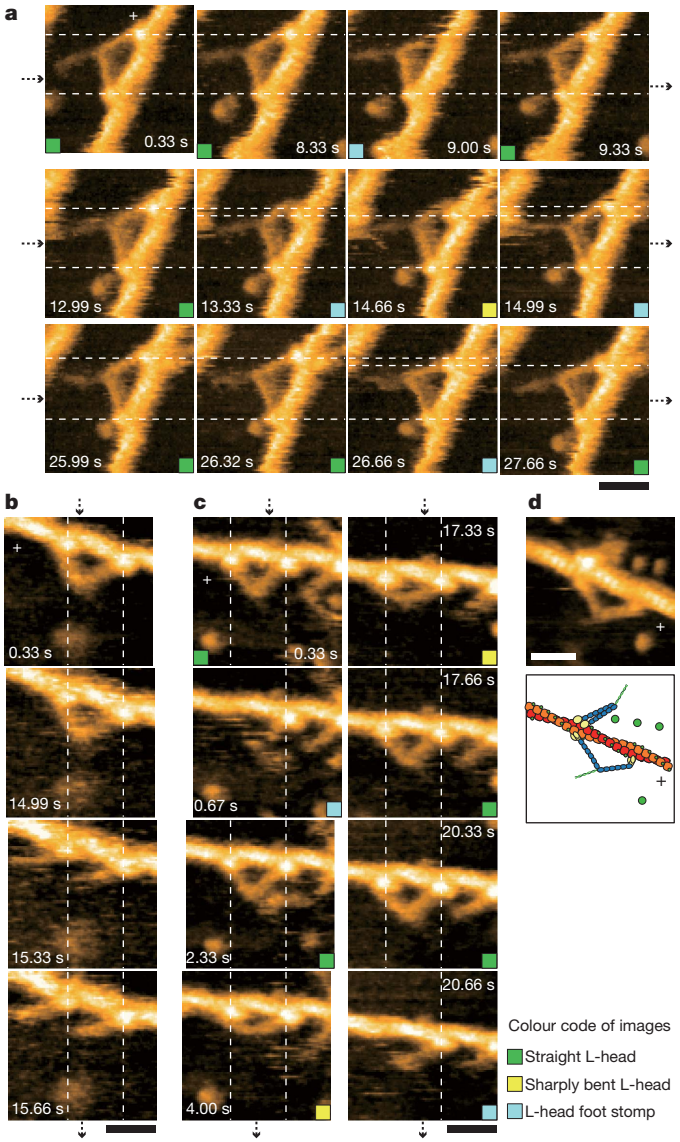

Figure 2 | AFM images of M5-HMM in ADP and under the nucleotide-free condition. **a**, Successive AFM images taken in 50 μM ADP (Supplementary Movie 3). **b**, Successive AFM images showing unwinding of the short coiled-coil tail of two-headed bound M5-HMM observed in 50 μM ADP (Supplementary Movie 4). **c**, Successive AFM images made under the nucleotide-free condition (Supplementary Movie 5). **d**, AFM image and illustration of nucleotide-free M5-HMM with heads bound to adjacent actin subunits. A plus sign is used to indicate the plus end of actin. All images were taken at 333.2 ms per frame with a scan size of 90×90 nm^2. Scale bars, 30 nm.

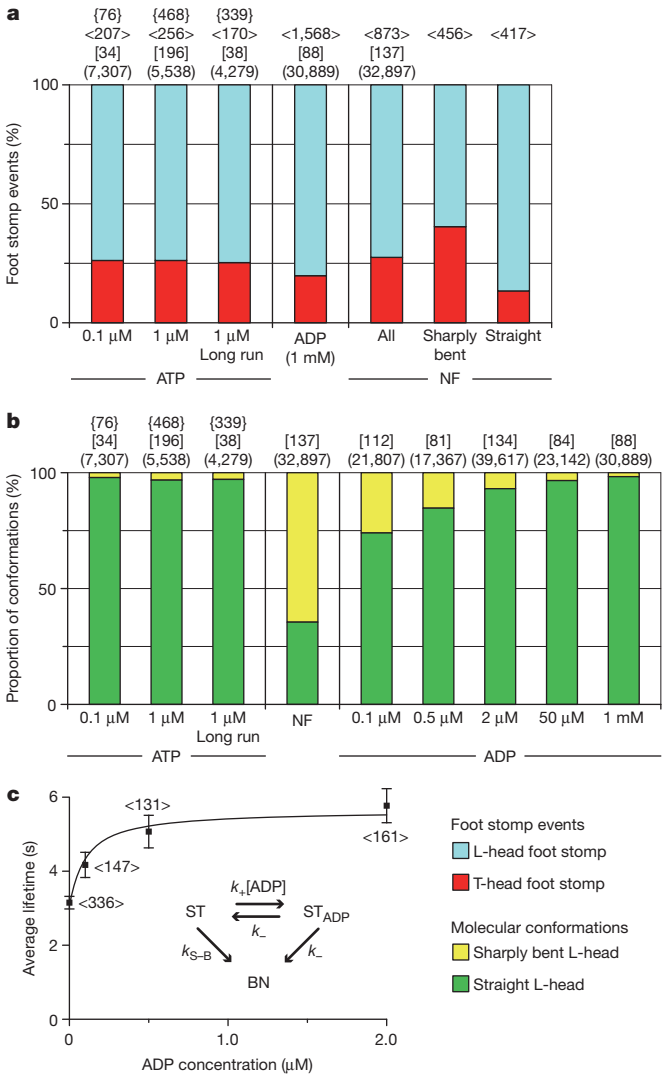

Figure 3 | Foot stomp and L-head conformations in different nucleotide conditions. **a**, **b**, Proportion of foot stomp frequencies observed at the L- and T-heads (**a**) and of the detected straight and sharply bent conformations of the L-head (**b**). The numbers of steps, events, molecules and frames examined using images within which both heads were fully located are enclosed in {curly}, <angle>, [square] and (round) brackets, respectively. 'Long run' represents data obtained using wide imaging areas. NF, nucleotide free. **c**, Average lifetimes of the L-head with a straight conformation for various [ADP] values. The total numbers of straight-to-bent transition events observed with ~50 different molecules under the respective [ADP] values are shown in angle brackets. Inset, reaction scheme (ST, nucleotide-free, straight L-head; ST_{ADP}, ADP-bound, straight L-head; BN, sharply bent, nucleotide-free L-head). Error bars, ±s.e.m.; $k_{S-B} = 0.32 \pm 0.02\ s^{-1}$ (best-fit value ± s.d.).

occurrence indicate that a foot stomp at the L-head occurs while it is bound to ADP, not while it is bound to ADP–P_i. If P_i release, the rate of which is independent of [ATP], were significantly delayed by the interaction of M5-HMM with the substrate surface containing 5% DPTAP, M5-HMM in high [ATP] would walk much more slowly than observed. Moreover, the foot stomp also occurs when DPTAP is absent from the substrate. A foot-stomp-like behaviour was previously suggested in a fluorescence microscopy observation of walking myosin V molecules[25]. Thus, the foot stomp is an inherent behaviour of myosin V. As will be described later, the foot stomp also occurs in ADP and under the nucleotide-free condition.

Conformational transition in the L-head

Even under the nucleotide-free condition, M5-HMM was bound to actin through the two heads (Fig. 2c, Supplementary Movie 5 and Supplementary Fig. 3c). However, unlike in the presence of nucleotides, the leading neck frequently had a sharply bent conformation and alternated back and forth between this conformation and the nearly straight conformation (Fig. 2c and Supplementary Fig. 3c), indicating that they are in equilibrium. The sharply bent conformation at the L-head was also observed recently by negative-stain electron microscopy of acto-M5-HMM, although the chemical state was unspecified[17]. In the sharply bent conformation, both heads have the ARH orientation around the motor domain; thus, both necks appear to emerge from the front of the respective motor domains. As will be clarified later, this sharp bending has no relevance to power-stroke generation but provides a useful indicator of whether or not the L-head contains ADP.

The proportions of the straight L-head detected (r) were 0.98 in 1 mM ADP and 0.36 under the nucleotide-free condition (Fig. 3b). This finding is consistent with the ARH orientation distributions of single-headed

myosin V under the nucleotide-free and ADP-bound conditions (Supplementary Fig. 4). Under the nucleotide-free condition, the orientation angle relative to the long axis of the actin filament was $34 \pm 10^\circ$ (mean ± s.d.) (although a double-Gaussian distribution is somewhat significant: $33 \pm 9^\circ$ and $51 \pm 7^\circ$; *F*-test, $P < 0.05$). In ADP, however, the angle was distributed more widely ($29 \pm 11^\circ$ and $51 \pm 15^\circ$; *F*-test, $P < 10^{-6}$), which may be relevant to two different ADP-bound states in equilibrium[23]. Therefore, the hinge around the neck–motor domain junction of the ADP-bound head is more flexible than that of the nucleotide-free head. Because of the relatively rigid hinge of the nucleotide-free head, the leading neck in the R-ARH orientation tends to be sharply bent to release the large strain accumulated in the neck. This rigid hinge is also indicated by the observation that both heads are rarely bound to adjacent actin subunits predominantly in the nucleotide-free condition (Fig. 2d).

ADP release from the L-head

In 1 μM ATP and even in 0.1 μM ATP, the leading neck was mostly straight ($r \approx 0.98$) (Fig. 3b), which suggests that the L-head retains ADP until the T-head binds to ATP and detaches from actin, consistent with previous reports[14,26–30]. From the proportion (Fig. 3b) and lifetime (Fig. 3c and Supplementary Movie 6) of the straight L-head as a function of [ADP], we estimated the kinetic parameters for ADP binding/dissociation on the L-head: the ADP dissociation constant is $K_d = k_-/k_+ = 0.075 \pm 0.013$ μM; the ADP dissociation rate constant is $k_- = 0.100 \pm 0.004\ s^{-1}$; and the second-order ADP binding rate constant is $k_+ = 1.3 \pm 0.3\ \mu M^{-1}s^{-1}$. The value of k_- is ~70 times smaller than the corresponding rate for the T-head estimated above ($k_2 = 7.2 \pm 1.5\ s^{-1}$). This degree of asymmetry between the two heads is similar to that previously reported[26]. The value of k_+ is ~10 times smaller than the corresponding value, $12.6\ \mu M^{-1}\ s^{-1}$, previously measured in a solution study on single-headed myosin V[24]. The ADP dissociation rate constant of $0.100\ s^{-1}$ means that, on average, one ADP is released from the L-head every 10 s. However, M5-HMM walks many steps during 10 s. Thus, we confirm the consensus view that the sequential events of ADP release, the subsequent ATP binding and the resulting head dissociation take place solely at the T-head, which is the basis for the processivity and hand-over-hand stroke generation[14,26–30]. Accordingly, the sharp bending observed at the nucleotide-free L-head has no relevance to power-stroke generation.

Foot stomp in ADP and nucleotide-free conditions

The foot stomp observed in ATP also occurred with higher frequencies at the L-head under all the nucleotide conditions examined here (Fig. 3a, Supplementary Fig. 5 and Supplementary Movies 3 and 5). Note that in ADP and under the nucleotide-free condition, complete detachment of the T-head was only sometimes observed. This detachment was followed by a forward step. This event was also counted as a foot stomp. The foot stomp at the T-head mostly occurred as brief translocation along actin. The frequency difference between the two heads became smaller when the L-head assumed a sharply bent conformation (L-head/T-head frequency ratio, ~3:2). Thus, the frequency of foot stomping strongly correlates with the orientation of the bound head. Both heads would by nature preferentially take the ARH orientation. However, the nucleotide-bound L-head is forced to bind to actin in the R-ARH orientation and hence tends to detach from actin, leading to more frequent foot stomping. This implies that the L-head would be less susceptible to catalytic activation by actin, possibly contributing to some extent to the asymmetry in the kinetic constants between the two heads.

Discussion

In general, the conformational change in myosin upon the hydrolysis of bound ATP to ADP–P_i is the recovery stroke (that is, the post-stroke-to-pre-stroke transition), and the actin-activated P_i release from ADP–P_i reverses the head conformation to produce a forward force[23]. However, a forward force (or the strained pre-stroke state) can also be produced by the direct binding of the ADP-bound L-head to actin. In ATP, the force that is produced in this way after a foot stomp at the L-head drives lever-arm swing. The number of foot stomp events at the L-head per step is around one only for low [ATP]. However, this type of force generation is likely to take place also for high [ATP] under a loaded condition. Moreover, this force generation mechanism suggests that the ADP-bound head has the potential to produce a force repeatedly when an appropriate backward force is applied. This potential was recently indicated in an optical-trap-based experiment on a single myosin V head interacting with actin under a certain backward load[31]. The power stroke is reversed and actin-bound pre- and post-stroke conformations are repeated before one ATPase cycle is completed. In Supplementary Fig. 6, we propose a model for the chemomechanical cycle of myosin V based on previous studies and the new findings obtained here.

As demonstrated here, previously known and unknown behaviours of M5-HMM clearly appear in the molecular movies. Unlike previous methods, high-resolution HS-AFM imaging unselectively provides comprehensive information on the structure and dynamics of a functioning molecule. Thus, the HS-AFM imaging of functioning biomolecules has the potential to transform the fields of structural biology and single-molecule biology.

METHODS SUMMARY

We prepared M5-HMM from chick brain, and prepared partially biotinylated actin filaments and stabilized them with phalloidin[11]. Biotin-containing lipid bilayers were formed on a mica surface[8]. We immobilized the biotinylated actin filaments on the bilayer surface and then deposited a solution of M5-HMM on the surface. All imaging experiments were performed in the tapping mode using a laboratory-built HS-AFM apparatus[2,3].

Full Methods and any associated references are available in the online version of the paper at www.nature.com/nature.

Received 3 June; accepted 24 August 2010.
Published online 10 October 2010.

1. Joo, C. *et al.* Advances in single-molecule fluorescence methods for molecular biology. *Annu. Rev. Biochem.* **77,** 51–76 (2008).
2. Ando, T., Uchihashi, T. & Fukuma, T. High-speed atomic force microscopy for nano-visualization of dynamic biomolecular processes. *Prog. Surf. Sci.* **83,** 337–437 (2008).
3. Ando, T. *et al.* A high-speed atomic force microscope for studying biological macromolecules. *Proc. Natl Acad. Sci. USA* **98,** 12468–12472 (2001).
4. Hansma, P. K., Schitter, G., Fantner, G. E. & Prater, C. High-speed atomic force microscopy. *Science* **314,** 601–602 (2006).
5. Viani, M. B. *et al.* Probing protein–protein interactions in real time. *Nature Struct. Biol.* **7,** 644–647 (2000).
6. Shibata, M. *et al.* High-speed atomic force microscopy shows dynamic molecular processes in photoactivated bacteriorhodopsin. *Nature Nanotechnol.* **5,** 208–212 (2010).
7. Yamashita, H. *et al.* Dynamics of bacteriorhodopsin 2D crystal observed by high-speed atomic force microscopy. *J. Struct. Biol.* **167,** 153–158 (2009).
8. Yamamoto, D., Uchihashi, T., Kodera, N. & Ando, T. Anisotropic diffusion of point defects in a two-dimensional crystal of streptavidin observed by high-speed atomic force microscopy. *Nanotechnology* **19,** 384009 (2008).
9. Sellers, J. R. & Weisman, L. S. in *Myosins: A Superfamily of Molecular Motors, Proteins and Cell Regulation* (ed. Coluccio, L.) 289–324 (Springer, 2008).
10. Mehta, A. D. *et al.* Myosin-V is a processive actin-based motor. *Nature* **400,** 590–593 (1999).
11. Sakamoto, T., Amitani, I., Yokota, E. & Ando, T. Direct observation of processive movement by individual myosin V molecules. *Biochem. Biophys. Res. Commun.* **272,** 586–590 (2000).
12. Yildiz, A. *et al.* Myosin V walks hand-over-hand: single fluorophore imaging with 1.5 nm localization. *Science* **300,** 2061–2065 (2003).
13. Forkey, J. N. *et al.* Three-dimensional structural dynamics of myosin V by single-molecule fluorescence polarization. *Nature* **422,** 399–404 (2003).
14. Sakamoto, T. *et al.* Direct observation of the mechanochemical coupling in myosin Va during processive movement. *Nature* **455,** 128–132 (2008).
15. Walker, M. L. *et al.* Two-headed binding of a processive myosin to F-actin. *Nature* **405,** 804–807 (2000).
16. Burgess, S. *et al.* The prepower stroke conformation of myosin V. *J. Cell Biol.* **159,** 983–991 (2002).
17. Oke, O. A. *et al.* Influence of lever structure on myosin 5a walking. *Proc. Natl Acad. Sci. USA* **107,** 2509–2514 (2010).
18. Baker, J. E. *et al.* Myosin V processivity: multiple kinetic pathways for head-to-head coordination. *Proc. Natl Acad. Sci. USA* **101,** 5542–5546 (2004).

19. Huxley, H. E. The mechanism of muscular contraction. *Science* **164,** 1356–1366 (1969).
20. Hua, W., Chung, J. & Gelles, J. Distinguishing inchworm and hand-over-hand processive kinesin movement by neck rotation measurements. *Science* **295,** 844–848 (2002).
21. Okada, T. *et al.* The diffusive search mechanism of processive myosin class-V motor involves directional steps along actin subunits. *Biochem. Biophys. Res. Commun.* **354,** 379–384 (2007).
22. Wang, F. *et al.* Effect of ADP and ionic strength on the kinetic and motile properties of recombinant mouse myosin V. *J. Biol. Chem.* **275,** 4329–4335 (2000).
23. Geeves, M. A. & Holmes, K. C. Structural mechanism of muscle contraction. *Annu. Rev. Biochem.* **68,** 687–728 (1999).
24. De La Cruz, E. M. *et al.* The kinetic mechanism of myosin V. *Proc. Natl Acad. Sci. USA* **96,** 13726–13731 (1999).
25. Syed, S. *et al.* Adaptability of myosin V studied by simultaneous detection of position and orientation. *EMBO J.* **25,** 1795–1803 (2006).
26. Rosenfeld, S. S. & Sweeney, H. L. A model of myosin V processivity. *J. Biol. Chem.* **279,** 40100–40111 (2004).
27. Veigel, C., Schmitz, S., Wang, F. & Sellers, J. R. Load-dependent kinetics of myosin-V can explain its high processivity. *Nature Cell Biol.* **7,** 861–869 (2005).
28. Oguchi, Y. *et al.* Load-dependent ADP binding to myosins V and VI: implications for subunit coordination and function. *Proc. Natl Acad. Sci. USA* **105,** 7714–7719 (2008).
29. Purcell, T. J., Sweeney, H. L. & Spudich, J. A. A force-dependent state controls the coordination of processive myosin V. *Proc. Natl Acad. Sci. USA* **102,** 13873–13878 (2005).
30. Forgacs, E. *et al.* Kinetics of ADP dissociation from the trail and lead heads of actomyosin V following the power stroke. *J. Biol. Chem.* **283,** 766–773 (2008).
31. Sellers, J. R. & Veigel, C. Direct observation of the myosin-Va power stroke and its reversal. *Nature Struct. Mol. Biol.* **17,** 590–595 (2010).

Supplementary Information is linked to the online version of the paper at www.nature.com/nature.

Acknowledgements We thank T. Uchihashi and H. Yamashita for technical assistance and discussion, and J. Sellers for critical reading of the draft and for comments. This work was supported by CREST/JST, Special Coordination Funds for Promoting Science and Technology (Effective Promotion of Joint Research with Industry, Academia, and Government) from JST, a Grant-in-Aid for Basic Research (S) from JSPS, and Knowledge Cluster/MEXT–Japan.

Author Contributions N.K. performed the HS-AFM experiments and data analysis and wrote the first draft of the manuscript. D.Y. and N.K. developed the lipid-bilayer-based assay system. R.I. participated in the sample preparations in the early stage of this study. T.A. and N.K. developed the HS-AFM apparatus. T.A. designed the experiment and prepared the final manuscript.

Author Information Reprints and permissions information is available at www.nature.com/reprints. The authors declare no competing financial interests. Readers are welcome to comment on the online version of this article at www.nature.com/nature. Correspondence and requests for materials should be addressed to T.A. (tando@kenroku.kanazawa-u.ac.jp).

METHODS

Protein purification and reagents. We prepared M5-HMM from chick brain[32]. Partially biotinylated (20%) actin filaments were prepared and then stabilized with phalloidin[11]. Streptavidin, synthetic lipids, apyrase and hexokinase were purchased from Wako Pure Chemical, Avanti Polar Lipids, Sigma-Aldrich and Roche Diagnostics, respectively.

Preparation of samples for AFM observation. We formed biotin-containing lipid bilayers on a mica surface[8,33]. A typical lipid composition was 1,2-dipalmitoyl-*sn*-glycero-3-phosphocholine (DPPC), 1,2-dipalmitoyl-3-trimethylammonium-propane (DPTAP) and 1,2-dipalmitoyl-*sn*-glycero-3-phosphoethanolamine-*N*-(cap biotinyl) (biotin-cap-DPPE) in a weight ratio of 0.85:0.05:0.1. In some cases, the content of the positively charged lipid DPTAP was reduced. After rinsing the lipid bilayer substrate with buffer A (20 mM imidazole-HCl (pH 7.6), 25 mM KCl, 2 mM $MgCl_2$, 1 mM EGTA, 5 mM DTT), we deposited a drop (2 μl) of streptavidin in buffer A (10 nM) on the substrate for 3 min. In some experiments, additional streptavidin molecules (2 μl, 40 nM) were deposited on the surface for 2 min. After rinsing with buffer A, we deposited a drop (2 μl) of partially biotinylated actin filaments (1 μM) in buffer A on the lipid bilayers for 10 min. After rinsing with a solution containing either 0.1 μM to 1 mM ATP, 0.1 μM to 1 mM ADP (1 U ml^{-1} hexokinase and 10 mM glucose were added in the case of 1 mM ADP to remove contaminating ATP) or 1 U ml^{-1} apyrase (to ensure the nucleotide-free condition) in buffer A, we deposited a drop (2 μl) of the same solution plus M5-HMM (0.1 to 1 nM) on the lipid bilayers for 3 min. Finally, the sample was attached to the scanning stage of a HS-AFM apparatus and immersed in the same solution (~60 μl) without M5-HMM. When the lipid bilayers did not contain the positively charged lipid DPTAP, we further added M5-HMM to the observation solution.

HS-AFM apparatus and cantilevers. We used a laboratory-built tapping-mode HS-AFM apparatus[2,3] together with small cantilevers designed for HS-AFM[3,4] (spring constant, 0.1–0.2 N m^{-1}; resonant frequency in water, 0.8–1.2 MHz; quality factor in water, ~2). The probe tip was grown on the tip of a cantilever by electron-beam deposition and was further sharpened by argon plasma etching[2]. In the best case, a tip apex radius of ~4 nm was achieved. To achieve a small tip–sample loading force, the free-oscillation peak-to-peak amplitude of the cantilever (A_0) was set to 1.5–2.5 nm and the amplitude set point was set at more than $0.9A_0$. We note that the mechanical quantity that affects the sample is not the force itself but the force impulse, that is, the product of force and the time over which the force acts. In tapping-mode HS-AFM, the time of force action is short (~100 ns) and, therefore, a relatively large peak force (~20 pN) would not affect the sample significantly. All the imaging experiments could be routinely conducted without difficulty except for the occasional deterioration of image quality owing to tip smear or cracking, which was difficult to control. The tip smearing was caused by the attachment of molecules contained in the sample, but they were sometimes removed during imaging. The cracking of the sharp tip yields a double image of every object, as shown in Supplementary Movie 6.

HS-AFM imaging and processive run. All observations were performed at room temperature (24–26 °C). To facilitate rapid imaging of moving M5-HMM molecules on actin, we chose sample areas in which actin filaments were aligned approximately parallel to the *x* direction. Myosin V walks approximately straight along actin filaments as the two heads span the filament's helical pseudorepeat of ~36 nm (refs 10, 12–15). This property and the high-precision feedback system of the instrument[2,35] facilitate the continuous imaging of walking M5-HMM molecules weakly adsorbed sideways onto the DPTAP-containing substrate surface. In the absence of DPTAP in the substrate, M5-HMM molecules often walked on the top surface of actin filaments. In this case, it was difficult to acquire high-resolution images because AFM is inefficient for visualizing molecules not supported on a surface.

High-resolution imaging of moving M5-HMM. To obtain high-resolution images of M5-HMM molecules translocating along actin in 0.1–2 μM ATP, the scan area was narrowed (typically to about $130 \times 65\ nm^2$) and the number of pixels was optimized (80×40 or 80×50) such that the phase delay in tracing the sample surface was minimized and the imaging rate (146.7 ms per frame) was high enough to capture the moving molecules. When long processive runs (~15 steps) in 0.1–2 μM ATP were observed, the molecules were tracked by shifting the narrow scan area manually (mainly in the *x* direction). The tracking sometimes could not be continued when the target molecule collided with a molecule walking ahead, when a portion of discontinuous substrate surface was encountered or when the manual tracking by an operator was not appropriately made. The occasional failure of continual tracking is not due to the tip–sample interaction.

Velocity measurements. In the experiment to determine the translocation velocity of M5-HMM for various [ATP] values, we fixed the scan areas ($400 \times 125\ nm^2$) and captured images at 146.3 ms per frame. To facilitate rapid imaging of this relatively wide scan area, the number of pixels was reduced to 80×25 (thus, the scan velocity in the *x* direction is only slightly higher than that in high-resolution imaging mentioned above). The image quality was generally lowered but was high enough to identify M5-HMM molecules on actin. When the velocity of a translocating molecule was high, some of the dwell events could not be detected. In this case, we determined it using at least four different dwell positions where the molecule being tracked was captured on video.

Imaging for detecting foot stomp and L-head conformations. In the experiment to analyse foot stomping and L-head conformations in ADP and under the nucleotide-free conditions, we carried out the imaging at 333.2 ms per frame using fixed imaging areas (typically $90 \times 90\ nm^2$ with 80×80 pixels). In the experiment to analyse foot stomping and L-head conformations in ATP, the imaging was carried out at 146.7 ms per frame using two scan modes. In one mode, the imaging areas were fixed (typically at $130 \times 65\ nm^2$ with 80×40 pixels). M5-HMM molecules that entered the imaging areas were captured on video. In the other mode, a translocating M5-HMM molecule was tracked by shifting the scan area (typically $130 \times 65\ nm^2$ with 80×40 pixels).

Image analysis. We applied to each AFM image a Gaussian filter for removing spike noises and a flattening filter for removing the substrate-tilt effect. Each position of the motor domain of M5-HMM was determined by calculating the centre of mass to measure its displacement. The following events were considered as a foot stomp: (1) an entire head disappears and then reappears at approximately the same position; (2) either motor domain of a two-headed bound M5-HMM molecule is translocated by around ±5 nm along the actin filament; and (3) a motor domain disappears while its neck domain is visible (that is, the head detaches while scanning the region where the motor domain was attached in the previous frame scan, and then rebinds to actin). Moreover, when an entire T-head disappeared in ADP and under the nucleotide-free condition, the molecule sometimes stepped forward. This event was also counted as a foot stomp. We note that a foot stomp was also observed even when the substrate surface did not contain DPTAP, although we did not systematically analyse this. When the L-head is sharply bent, the neck–neck junction becomes closer to the bound actin filament (and, hence, the space surrounded by the two heads and actin becomes narrower). We identified the sharply bent conformation by visual observation of these features. For the quantitative analysis of foot stomp events and L-head conformations in ATP, we analysed only images within which both heads were fully located before and after a step. Therefore, we observed more steps than are shown in Fig. 3a, b.

Kinetic analysis of conformational change at L-head. We analysed the proportion of the straight L-head conformation detected (*r*) as a function of [ADP] (Fig. 3b) to estimate the ADP dissociation constant for the L-head (K_d) using the relationship

$$r([\mathrm{ADP}]) = \frac{r_D[\mathrm{ADP}] + r_{NF}K_d}{[\mathrm{ADP}] + K_d}$$

where $r_D = 0.98$ and $r_{NF} = 0.36$ are the proportions of straight L-head detected in a saturating amount of ADP and under the nucleotide-free condition, respectively. Considering the reaction scheme (Fig. 3c, inset), the average lifetime of the straight L-head, $\langle \tau_{ST} \rangle$, is expressed approximately as

$$\langle \tau_{ST} \rangle = n_{NF}\left(k_{S-B} + \frac{k_-k_+[\mathrm{ADP}]}{k_- + k_+[\mathrm{ADP}]}\right)^{-1} + n_{ADP}\left(k_- + \frac{k_-k_{S-B}}{k_- + k_{S-B}}\right)^{-1} \quad (1)$$

where k_{S-B} represents the spontaneous straight-to-bent transition rate for the nucleotide-free L-head; n_{NF} and n_{ADP} are the fractions of nucleotide-free L-head and ADP-bound L-head for a given [ADP] value, respectively, which are calculated using $K_d = 0.075$ μM; and k_- and k_+ are the ADP dissociation rate constant and ADP association rate constant at the L-head, respectively. Using equation (1), the observed $\langle \tau_{ST} \rangle$ as a function of [ADP] (Fig. 3c) was analysed to estimate k_{S-B}, k_- and k_+.

32. Koide, H. *et al.* Identification of the single specific IQ motif of myosin V from which calmodulin dissociates in the presence of Ca^{2+}. *Biochemistry* **45,** 11598–11604 (2006).
33. Yamamoto, D. *et al.* High-speed atomic force microscopy techniques for observing dynamic biomolecular processes. *Methods Enzymol.* **475,** 541–564 (2010).
34. Kitazawa, M., Shiotani, K. & Toda, A. Batch fabrication of sharpened silicon nitride tips. *Jpn. J. Appl. Phys.* **42,** 4844–4847 (2003).
35. Kodera, N., Sakashita, M. & Ando, T. Dynamic proportional-integral-differential controller for high-speed atomic force microscopy. *Rev. Sci. Instrum.* **77,** 083704 (2006).